

Smart Grid Monitoring Using Power Line Modems: Effect of Anomalies on Signal Propagation

Federico Passerini, *Student Member, IEEE*, and Andrea M. Tonello, *Senior Member, IEEE*

Abstract—The aim of the present work is to provide the theoretical fundamentals needed to monitor power grids using high frequency sensors. In our context, network monitoring refers to the harvesting of different kinds of information: topology of the grid, load changes, presence of faults and cable degradation. We rely on transmission line theory to carry out a thorough analysis of how high frequency signals, such those produced by power line modems, propagate through multi-conductor power networks. We also consider the presence of electrical anomalies on the network and analyze how they affect the signal propagation. In this context, we propose two models that rely on reflectometric and end-to-end measurements to extrapolate information about possible anomalies. A thorough discussion is carried out to explain the properties of each model and measurement method, in order to enable the development of appropriate anomaly detection and location algorithms.

Index Terms—Smart Grid, Network monitoring, Fault Detection, Cable Aging, Topology Derivation, Grid Anomalies

I. INTRODUCTION

HIGH frequency monitoring is an essential tool to operate modern distribution grids, since it allows the utilities to sense different kind of electrical events that will or potentially can alter the status of the network. While monitoring is traditionally performed using phasor measurement units (PMUs) [1], other devices that can operate at high frequency are nowadays more and more deployed in distribution grids, e.g. power line modems (PLMs).

PLMs are conventionally used as communication devices in smart grids (SGs) [2], [3] but, as shown in this paper, can also serve as network monitoring devices. This role is similar to that of DSL Access Multiplexers (DSLAMs) in local loops, for which considerable amount of research has been carried out (see [4], [5], [6] and references therein). However, the power line medium is rather different from the twisted pair loops used in DSL, especially when considering distribution grids. In fact, while DSL loop cables are standardized for high speed communications, power line cables are not; the topological structure of power line networks changes rather often, while DSL networks have constant topologies; the loads of distribution networks have convoluted frequency profiles and are time variant, while DSL loads are constant in time and have values close to the line impedance. Most importantly, the focus in DSL is about providing high speed internet to the users, so the main interest of the DSL engineers is to qualify the loop and to detect bad splices or possible short circuits. The main interest in power distribution networks is, conversely, to

deliver energy in an optimized and reliable way. This means that it is not only important to identify poor connections and short circuits, but to prevent them, in order to avoid power cuts that might cause severe problems to the local community. Wake-up calls in this context are generated by high impedance faults (HIF) or by the detection of cable aging due to water treeing, oxidation and other causes. These events that we name anomalies cause almost undetectable damage to the network, but on a medium to long run can cause a complete system failure. Different techniques have been proposed to detect and locate anomalies, which involve measurements at the mains frequency and its harmonics up to few kHz, using either pulsed, sinusoidal or wavelet test signals [7], [8].

In recent years, relevant research has been carried out to analyze what information can be harvested about a power line network (PLN) using signals from 3 kHz up to 86 MHz, which are typical of power line communications (see [9], [10], [11] and references therein). These works rely on the signal generation and acquisition capabilities of PLMs to sense the grid. Since the research in this area is still in early stage, there is a need to establish a solid theoretical foundation about the information carried by high frequency signals in PLNs.

This paper is dedicated to provide a detailed answer to this requirement. To this aim, we rely on transmission line theory [12] and derive closed-form relations that describe the overall effect of the network on three different quantities: the impedance and the reflection coefficient measured at one node (reflectometric sensing), and the channel transfer function (CTF) of a signal coming from a far-end node (end-to-end sensing). The differences between these relations allow us to highlight the information about the network status carried by each of the aforementioned quantities. Afterwards, we introduce the presence of electrical anomalies and analytically study how they affect the propagation of high-frequency signals. In this context, we present two models that allow us to separate the information relative to the anomaly from the information relative to the rest of the network. We discuss the differences between these two models and also analyze which information about the anomaly can each of the considered quantities provide.

The analysis presented in this paper can be used, as done in [13], to propose efficient modem architectures and post-processing algorithms to detect, classify and locate anomalies.

The rest of the paper is organized as follows. In Section II we provide new insights about the theory that describes the propagation of signals in power line networks. In Section III we analyze how the presence of an anomaly alters the propagation of both end-to-end and reflectometric signals. Conclusions follow in Section IV.

Federico Passerini and Andrea M. Tonello are with the Embedded Communication Systems Group, University of Klagenfurt, Klagenfurt, Austria, e-mail: {federico.passerini, andrea.tonello}@aau.at.

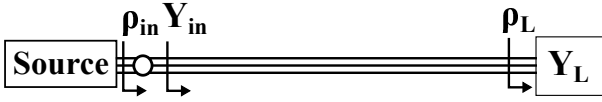


Fig. 1. Example of a single MTL connecting a signal generator and a load.

II. PROPAGATION OF HIGH FREQUENCY SIGNALS IN PLNS

The propagation of high frequency signals in PLNs is generally described by the multiconductor transmission line (MTL) theory [12]. In this section, we introduce some new theoretical insights of this theory that are needed to relate the input admittance, the input reflection coefficient and the CTF to the network parameters.

Let us consider a single MTL that links a signal generator, which can be a PLM, and a load described by its admittance matrix \mathbf{Y}_L of size $L \times L$, where L is the number of conductors (see Fig. 1). The propagation of the signal is described by the telegraph equations

$$\begin{aligned} \frac{\partial \mathbf{V}(x, f)}{\partial x} &= -(\mathbf{R} + j2\pi f \mathbf{L}) \mathbf{I}(x, f) \\ \frac{\partial \mathbf{I}(x, f)}{\partial x} &= -(\mathbf{G} + j2\pi f \mathbf{C}) \mathbf{V}(x, f) \end{aligned} \quad (1)$$

where \mathbf{V} and \mathbf{I} are the voltage and current vectors respectively, x is the distance from the load, $\{\mathbf{R}, \mathbf{L}, \mathbf{G}, \mathbf{C}\}$ is the set of matrices that describes the per unit length parameters of the cable and f is the considered frequency. The dependency on the frequency will be omitted in the following to simplify the notation.

A. Analysis of the reflectometry

The input admittance matrix \mathbf{Y}_{in} at the beginning of an MTL with length ℓ_1 can be written after some derivations as [14]

$$\mathbf{Y}_{in} = \mathbf{T} (\mathbf{I} + e^{-\Gamma \ell_1} \rho_L^M e^{-\Gamma \ell_1}) (\mathbf{I} - e^{-\Gamma \ell_1} \rho_L^M e^{-\Gamma \ell_1})^{-1} \mathbf{T}^{-1} \mathbf{Y}_C \quad (2)$$

where \mathbf{Y}_C and Γ are the characteristic admittance and the propagation constant of the cable respectively, \mathbf{T} is a transformation matrix, \mathbf{I} is the identity matrix, and ρ_L is the load reflection coefficient matrix defined as

$$\rho_L = \mathbf{Y}_C (\mathbf{Y}_L + \mathbf{Y}_C)^{-1} (\mathbf{Y}_L - \mathbf{Y}_C) \mathbf{Y}_C^{-1} \quad (3)$$

respectively. We also name ρ_L^M the modal load reflection coefficient, where $\rho_L^M = \mathbf{T}^{-1} \rho_L \mathbf{T}$. In general, the relation between a modal matrix \mathbf{A}^M and its non-modal counterpart \mathbf{A} is

$$\mathbf{A}^M = \mathbf{T}^{-1} \mathbf{A} \mathbf{T}.$$

The input reflection coefficient matrix ρ_{in} is defined as [12]

$$\rho_{in} = \mathbf{Y}_R (\mathbf{Y}_{in} + \mathbf{Y}_R)^{-1} (\mathbf{Y}_{in} - \mathbf{Y}_R) \mathbf{Y}_R^{-1} \quad (4)$$

where \mathbf{Y}_R is the generator admittance matrix at the signal generator side. Combining (2) and (4), we obtain

$$\rho_{in} = \mathbf{N} \mathbf{T} (\rho_G^M + \rho_B^M) (\mathbf{I} + \rho_G^M \rho_B^M)^{-1} \mathbf{T}^{-1} \mathbf{N}^{-1} \quad (5)$$

where $\mathbf{N} = (\mathbf{Y}_R + \mathbf{Y}_C) \mathbf{Y}_C^{-1}$ and ρ_G^M is the modal line mismatch coefficient matrix defined as

$$\rho_G^M = \mathbf{T}^{-1} \mathbf{Y}_C (\mathbf{Y}_C + \mathbf{Y}_R)^{-1} (\mathbf{Y}_C - \mathbf{Y}_R) \mathbf{Y}_C^{-1} \mathbf{T} \quad (6)$$

and ρ_B^M is the modal reflection coefficient matrix computed at the signal generator side of the line, defined as

$$\rho_B^M = e^{-\Gamma \ell_1} \rho_L^M e^{-\Gamma \ell_1}. \quad (7)$$

We remark that (2) and (5) are a multidimensional extension of the scalar input admittance and input reflection coefficient equations [5, Ch. 2], of which they preserve the structure. Finally, the echo signal coming back to the signal source from the MTL is given by

$$\mathbf{V}_{echo} = -\mathbf{Y}_R^{-1} \rho_{in} \mathbf{Y}_R \mathbf{V}_{source}. \quad (8)$$

In order to derive some useful insights about (2) and (5), we make use of the fact that the Taylor series of any invertible square matrix $(\mathbf{I} + \mathbf{A})^{-1}$ is [15]

$$(\mathbf{I} + \mathbf{A})^{-1} = \mathbf{I} + \sum_{n=1}^{\infty} (-1)^n \mathbf{A}^n.$$

The inversion is possible when the absolute value of all the eigenvalues of \mathbf{A} is less than one. Considering now $\mathbf{A} = e^{-\Gamma x} \rho_L^M e^{-\Gamma x}$, its eigenvalues can in principle be greater than one since any component of ρ_L^M can be greater than one [16]. However, we suppose that the magnitude of the eigenvalues of ρ_L^M is sufficiently damped by the exponential matrices, which is normally the case in PLNs. The input admittance matrix (2) can be therefore rewritten as

$$\mathbf{Y}_{in} = \mathbf{T} \left[\mathbf{I} + 2 \sum_{n=1}^{\infty} (e^{-\Gamma \ell_1} \rho_L^M e^{-\Gamma \ell_1})^n \right] \mathbf{T}^{-1} \mathbf{Y}_C \quad (9)$$

and (5) can be rewritten as

$$\begin{aligned} \rho_{in} &= \mathbf{N} \mathbf{T} \rho_G^M \mathbf{T}^{-1} \mathbf{N}^{-1} + \mathbf{N} \mathbf{T} \left[(\mathbf{I} - \rho_G^M \rho_B^M) e^{-\Gamma \ell_1} \right. \\ &\quad \left. \rho_L^M e^{-\Gamma \ell_1} \sum_{n=0}^{\infty} (-1)^n (\rho_G^M e^{-\Gamma \ell_1} \rho_L^M e^{-\Gamma \ell_1})^n \right] \mathbf{T}^{-1} \mathbf{N}^{-1}. \end{aligned} \quad (10)$$

(9) and (10) are composed by the sum of three elements: a constant w.r.t. ℓ_1 , a first exponential function depending on $2\ell_1$, and an infinite series of exponentials depending on multiples of this distance. We now make use of the matrix inverse Fourier transform defined for any \mathbf{X} matrix as

$$\mathbf{x}(t) = \int_{-\infty}^{+\infty} \mathbf{X}(f) e^{j2\pi f t} df, \quad (11)$$

and apply it to (9) and (10). The resulting multidimensional time traces are

$$\begin{aligned} \mathbf{y}_{in}(t) &= \left[\delta(t) * \mathbf{e}_0 * \delta(t) \right. \\ &\quad \left. + 2 \sum_{n=1}^{\infty} \delta(t - 2n\tau_1) * \mathbf{e}_n * \delta(t - 2n\tau_1) \right] * \mathbf{y}_{C_1}(t) \end{aligned} \quad (12)$$

and

$$\rho_{\text{in}}(t) = \delta(t) * \mathbf{f}_0 * \delta(t) + \sum_{n=1}^{\infty} \delta(t - 2\mathbf{t}_1) * \mathbf{f}_n * \delta(t - 2n\mathbf{t}_1) \quad (13)$$

where $*$ denotes the matrix-wise convolution operation, \mathbf{e}_n and \mathbf{f}_n denote functions that depend on time but not on the position of the nodes, $\delta(t)$ is a diagonal matrix whose elements are delta functions and \mathbf{t}_1 is a vector of propagation times (the propagation velocities over the different conductor pairs might be different) between the signal source and the load. We point out that $\mathbf{e}_0 = \mathbf{I}$ and $\mathbf{f}_0 = \mathbf{N}\rho_{\mathbf{G}}\mathbf{N}^{-1}$, so the envelope of the first peak depends only on $\mathbf{y}_{\mathbf{C}_1}$ and its eventual mismatch with $\mathbf{Y}_{\mathbf{R}}$.

If we suppose constant propagation velocity \mathbf{v} and $\Gamma(f) = \Gamma_1 f$, where f is the frequency, then $\mathbf{t}_1 = \Gamma_1 \ell_1$. This case applies for ideal TLs, but in practical scenarios Γ might not have a direct proportionality to f [17]. More in general, we can write

$$\mathbf{t}_1 = \mathbf{g}(\Gamma_1, \ell_1), \quad (14)$$

where \mathbf{g} is a generic function.

We consider now a complex MTL network with a tree topology (no loops) made by N nodes and $N-1$ branches. The m th branch is characterized by its length ℓ_m and propagation matrix Γ_m . The input admittance matrix at the generator side can be expressed as (derivation in Appendix A)

$$\mathbf{Y}_{\text{in}} = \mathbf{T}_1 \left[\mathbf{I} + 2 \sum_{n=1}^N \prod_{m=1}^n \mathbf{A}_m e^{-\Gamma_m \ell_m} \prod_{m=0}^{n-1} \mathbf{B}_{n-m} e^{-\Gamma_{n-m} \ell_{n-m}} + 2 \sum_{n=N+1}^{\infty} \dots \right] \mathbf{T}_1^{-1} \mathbf{Y}_{\mathbf{C}_1} \quad (15)$$

and the input reflection coefficient matrix becomes

$$\rho_{\text{in}} = \mathbf{N}_1 \mathbf{T}_1 \left[\rho_{\mathbf{G}_1}^{\mathbf{M}} + \sum_{n=1}^N \prod_{m=1}^n \mathbf{C}_m e^{-\Gamma_m \ell_m} \prod_{m=0}^{n-1} \mathbf{D}_{n-m} e^{-\Gamma_{n-m} \ell_{n-m}} + \sum_{n=N+1}^{\infty} \dots \right] \mathbf{T}_1^{-1} \mathbf{N}_1^{-1} \quad (16)$$

where the subscript $_1$ refers to the line segment to which the signal source is branched and \mathbf{A}_m , \mathbf{B}_m , \mathbf{C}_m , \mathbf{D}_m are frequency dependent functions. We represented (15) and (16) in this form to highlight the fact that N components of the sum are a direct function of double the distance of each of the N nodes of the network from the signal generator. The sum proceeds to infinity with components that are functions of the first N terms. Finally, both \mathbf{Y}_{in} and ρ_{in} can be written in the more compact form

$$\mathbf{Y}_{\text{in}} = \mathbf{T}_1 \left[\sum_{n=1}^{\infty} \mathbf{E}_n e^{-\Gamma_{\text{eq}_n} \ell_{\text{eq}_n}} \right] \mathbf{T}_1^{-1} \mathbf{Y}_{\mathbf{C}_1} \quad (17)$$

and

$$\rho_{\text{in}} = \mathbf{N}_1 \mathbf{T}_1 \left[\rho_{\mathbf{G}_1}^{\mathbf{M}} + \sum_{n=1}^{\infty} \mathbf{F}_n e^{-\Gamma_{\text{eq}_n} \ell_{\text{eq}_n}} \right] \mathbf{T}_1^{-1} \mathbf{N}_1^{-1}, \quad (18)$$

where \mathbf{E}_n , \mathbf{F}_n are frequency dependent functions and the index n does not anymore refer to a branch but to a path instead. Consequently, ℓ_{eq} and Γ_{eq} are the length and the propagation constant of a specific propagation path (Γ_{eq} is not a diagonal matrix as Γ). In this form, (17) and (18) can be manipulated by standard frequency analysis tools to retrieve information about the parameters ℓ_{eq} , Γ_{eq} , \mathbf{E}_n and \mathbf{F}_n [18].

We now transform the aforementioned equations to the time domain by performing a multidimensional Fourier transform, which results in

$$\mathbf{y}_{\text{in}}(t) = \delta(t) * \mathbf{y}_{\mathbf{C}_1} * \delta(t) + 2 \sum_{n=1}^N \delta(t - 2\mathbf{t}_n) * \mathbf{e}_n * \delta(t - 2\mathbf{t}_n) + 2 \sum_{n=N+1}^{\infty} \dots \quad (19)$$

$$\mathbf{r}_{\text{in}}(t) = \delta(t) * \mathbf{r}_{\mathbf{G}_1} * \delta(t) + \sum_{n=1}^N \delta(t - 2\mathbf{t}_n) * \mathbf{f}_n * \delta(t - 2\mathbf{t}_n) + \sum_{n=N+1}^{\infty} \dots \quad (20)$$

where t_n is the flight time of the signal from the source to the n -th node, and $\mathbf{y}_{\mathbf{C}_1}$, \mathbf{r}_{in} and $\mathbf{r}_{\mathbf{G}_1}$ are the inverse Fourier transforms of $\mathbf{Y}_{\mathbf{C}_1}$, ρ_{in} and $\mathbf{N}_1 \mathbf{T}_1 \rho_{\mathbf{G}_1}^{\mathbf{M}} \mathbf{T}_1^{-1} \mathbf{N}_1^{-1}$ respectively. (19) and (20) show that the time domain reflectometric response of a MTL comprises a first signal starting at $t = 0$ which is generated by the impedance mismatch of the first line segment. This is followed by a series of smoothed peaks at $2\mathbf{t}_n$, $n \in 1 \dots N$ that identify the presence of the N nodes of the network. Another infinite series of peaks is summed up in the time trace, which are located at time instants that are linear combinations of the first N .

This information is commonly used when the topology of the network is not known. In fact, by converting time to distance, a reflectometric measurement gives information about the distance of all the network nodes from the measurement point. Different algorithms can be contextually exploited to merge this information and estimate the topology of the network (see for example [5], [4]).

Moreover, since the reflectometric frequency responses (15) and (16) are written as sums of damped exponentials, parametric models can be applied in special conditions in order to enhance the accuracy in the estimation of the position of the peaks (see for example [19]).

B. Analysis of the end-to-end propagation

The channel transfer function (CTF) \mathbf{H} of a single MTL cable with length ℓ_1 and a load $\mathbf{Y}_{\mathbf{L}}$ at the end can be written as [14]

$$\mathbf{H} = \mathbf{Y}_{\mathbf{C}}^{-1} \mathbf{T} (\mathbf{I} - \rho_{\mathbf{L}}) (\mathbf{I} - e^{-2\Gamma \ell_1} \rho_{\mathbf{L}})^{-1} e^{-\Gamma \ell_1} \mathbf{T}^{-1} \mathbf{Y}_{\mathbf{C}} \quad (21)$$

where the equivalence holds because Γ is a diagonal matrix. The voltage on the load results in

$$\mathbf{V}_{\mathbf{L}} = \mathbf{H} \mathbf{V}_{\text{source}}. \quad (22)$$

Using the same approach of the previous section, (21) can be rewritten as

$$\mathbf{H} = \mathbf{Y}_{\mathbf{C}}^{-1} \mathbf{T} (\mathbf{I} - \boldsymbol{\rho}_{\mathbf{L}}) \left[\sum_{n=0}^{\infty} (\mathbf{e}^{-2\Gamma \ell_1} \boldsymbol{\rho}_{\mathbf{L}})^n \right] \mathbf{e}^{-\Gamma \ell_1} \mathbf{T}^{-1} \mathbf{Y}_{\mathbf{C}}. \quad (23)$$

The corresponding time domain multidimensional trace is

$$\mathbf{h}(t) = \mathbf{y}_{\mathbf{C}_1}^{-1} * \sum_{n=0}^{\infty} \left[\delta(t - 2(n+1)\mathbf{t}_1) * \mathbf{a}_n * \delta(t - 2(n+1)\mathbf{t}_1) \right] * \mathbf{y}_{\mathbf{C}_1} \quad (24)$$

where \mathbf{a}_n is a time dependant matrix.

When a complex MTL network made by several different branches is considered, the chain rule of the CTF can be applied, so that the voltage on the load of the receiving end reads

$$\mathbf{V}_{\mathbf{L}} = \mathbf{H}_{\text{tot}} \mathbf{V}_{\text{source}}. \quad (25)$$

where

$$\mathbf{H}_{\text{tot}} = \prod_{n=1}^N \mathbf{H}_n = \prod_{n=1}^N \mathbf{Y}_{\mathbf{C}_n}^{-1} \mathbf{T}_n (\mathbf{I} - \boldsymbol{\rho}_{\mathbf{L}_n}) \left[\sum_{m=0}^{\infty} (\mathbf{e}^{-2\Gamma_n \ell_n} \boldsymbol{\rho}_{\mathbf{L}_n})^m \right] \mathbf{e}^{-\Gamma_n \ell_n} \mathbf{T}_n^{-1} \mathbf{Y}_{\mathbf{C}_n} \quad (26)$$

and $\boldsymbol{\rho}_{\mathbf{L}_n}$ is the equivalent reflection coefficient matrix at the end of each line segment. We remark that every \mathbf{H}_n is derived using the carry-back procedure presented in [20]. Finally, similarly to (17) and (18), \mathbf{H}_{tot} can be more in general written as

$$\mathbf{H}_{\text{tot}} = \sum_{n=1}^{\infty} \mathbf{A}_n \mathbf{e}^{-\Gamma_{\text{eq}_n} \ell_n}, \quad (27)$$

which allows thorough analysis of the transfer function using spectral analysis algorithms.

The product of exponential sequences in (26) becomes a convolution of delta functions in time domain. The time domain transfer function acquires the following form:

$$\mathbf{h}_{\text{tot}}(t) = \sum_{m=1}^{\infty} \delta \left(t - \sum_{n=1}^N p_{n,m} \mathbf{t}_n \right) * \mathbf{a}_{n,m} * \delta \left(t - \sum_{n=1}^N p_{n,m} \mathbf{t}_n \right), \quad (28)$$

where p_n is the number of times the signal has traveled through the n -th line segment. (28) represents an infinite series of smoothed pulses where the delay of each pulse is due to the total number of line segments the signal travels across before reaching the receiver. The number of possible paths is of course infinite, but it is important to remark that their spacing is, as for the reflectometry case, a function of the length of all the line segments in the network. Therefore, we might suppose that also end-to-end signals can be used with the aim of topology estimation. That is however not possible, due to the following

Theorem 1 (Time Domain Wide-Sense Symmetry). *When considering end-to-end propagation in a passive medium from point A to point B, the distance between each smoothed peak in the channel impulse response is the same as in the case of propagation from point B to point A, irrespective of the complexity of the scattering elements, their reflection coefficients, the impedance at the transmitter and at the receiver.*

An intuitive demonstration of Theorem 1 is given considering that the system is a two port passive network and, as all these kind of networks, it is reciprocal. A thorougher demonstration is given in Appendix B. We point out that the Theorem does not specify anything about the amplitude and the shape of the peaks. In fact, they are in general different when considering the A-to-B or B-to-A propagation paths. Because of Theorem 1, it is not possible to know whether a peak in the measured $\mathbf{h}_{\text{tot}}(t)$ identifies a node close to the near or the far end of the communication link. Hence, end-to-end communication cannot be used to reconstruct the topology of a network univocally. When applied to the case of anomaly estimation, the same principle applies. End-to-end communication can identify the distance of the anomaly, but there is always an ambiguity whether it is the distance from the transmitter or the receiver.

III. EFFECT OF ANOMALIES ON THE SIGNAL PROPAGATION

In this section, we present an analysis of the effect of electrical anomalies caused by faults or aged cables on the propagation of the signals in a PLN.

In a broad sense, an anomaly is a modification in the expected behavior of a system. In the case of SGs we identify three main categories of anomalies: concentrated faults, distributed faults and termination impedance changes. Both localized faults and impedance changes can be schematically represented as a Thevenin or Norton equivalent circuit that is superimposed at the fault location to the previously known system (see Fig. 2). In the literature, these circuits are normally reduced to a lumped impedance [9] or, equivalently, to a voltage or current generator [21]. On the other side, distributed faults like damaged cables, can only be represented by a cable section with modified parameters.

A. General models of the anomalies

The effect of such anomalies can be represented by an extra transfer function block \mathbf{A} inserted in the network chain model at the position of the anomaly occurrence (see Figure 3).

If we write the transfer function of branch j as $\mathbf{H}_j = \mathbf{H}_{j,1} \mathbf{H}_{j,0} \mathbf{H}_{j,2}$, in the presence of an anomaly on branch j , (26) becomes

$$\mathbf{H}_{\text{tot}_a} = \left(\prod_{n=1}^{j-1} \tilde{\mathbf{H}}_n \right) \tilde{\mathbf{H}}_{j,1} \mathbf{A} \mathbf{H}_{j,2} \left(\prod_{n=j+1}^N \mathbf{H}_n \right). \quad (29)$$

Here \mathbf{A} replaces $\mathbf{H}_{j,0}$, and $\tilde{\mathbf{H}}_{j,1}$ is equal to $\mathbf{H}_{j,1}$ where the load admittance is \mathbf{Y}_{in_A} instead of $\mathbf{Y}_{\text{in}_j,2}$. The modification of the load admittance is consequently propagated through all the $\tilde{\mathbf{H}}_n$, $n = 1 \dots j - 1$. When a load impedance change or

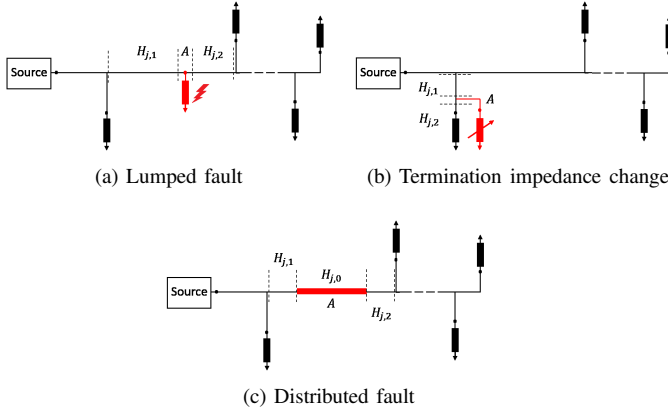


Fig. 2. Sketch of the electrical equivalent of different anomalies in a distribution network.

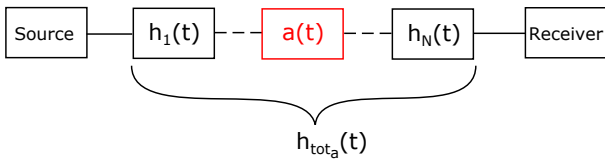


Fig. 3. Model of the anomaly using the chain representation.

a concentrated fault is considered, $\mathbf{H}_{j,0}$ is an identity matrix and \mathbf{A} is the transfer function of an impedance matrix. When a distributed fault is considered, $\mathbf{H}_{j,0}$ is the transfer function of the healthy cable and \mathbf{A} is the transfer function of the degraded cable. If we now want to obtain the CTF variation Δ_{ch}^H , which represents the compound effect of the anomaly on the network, we can compute the product

$$\mathbf{H}_{\text{tot}_a} \mathbf{H}_{\text{tot}}^{-1} = \left(\prod_{n=1}^{j,1} \tilde{\mathbf{H}}_n \right) \mathbf{A} \left(\prod_{n=0}^{(j,1)-1} \mathbf{H}_{(j,1)-n}^{-1} \right) = \Delta_{ch}^H. \quad (30)$$

Since the product from $j+1$ to N is the same in (26) and (29), the $N-j$ branches that are closest to the receiver are canceled out in (30). Hence, the system is reduced to a network whose closest node to the receiver is the one generated by the

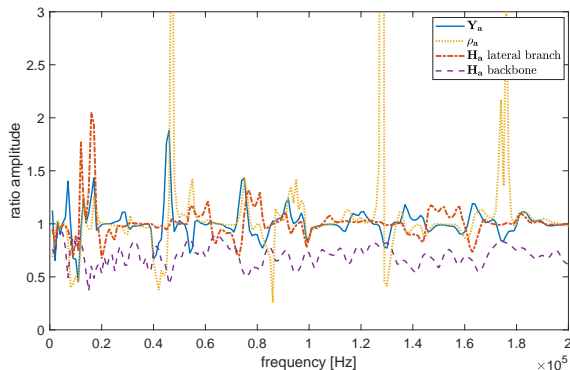


Fig. 4. Example of typical values obtained using the chain model. Two examples of \mathbf{H}_a are given: when the fault occurs on the backbone and when it occurs on a lateral branch.

anomaly. The first relevant exponential in Δ_{ch}^H is $e^{-2\Gamma_{eq}\ell_{eq_a}}$, where ℓ_{eq_a} is the distance of the beginning of the anomaly from the closest node to the anomaly. We point out that, if the anomaly is a fault and it occurs along the backbone, i.e. the direct path, between the transmitter and the receiver, it creates a further propagation path for the direct propagation wave, which in turn results in the reduction of the CTF. Conversely, when the anomaly occurs on a lateral branch, it does only affect secondary propagating waves, resulting on average in no signal loss (see Fig. (4)).

Considering now the case of the input admittance, starting from (17) we compute the admittance variation Δ_{ch}^Y as

$$\Delta_{ch}^Y = \mathbf{Y}_{\text{in}_a} \mathbf{Y}_{\text{in}}^{-1} = \mathbf{T}_1 \left[\sum_{m=1}^{\infty} \mathbf{E}_m e^{-\Gamma_{eq_m} \ell_{eq_m}} + \sum_{n=1}^{\infty} \mathbf{F}_n e^{-\Gamma_{eq_n} \ell_{eq_n}} \right] \left[\sum_{p=1}^{\infty} \mathbf{E}_p e^{-\Gamma_{eq_p} \ell_{eq_p}} \right]^{-1} \mathbf{T}_1^{-1}, \quad (31)$$

where the sum over n refers to the new paths caused by the anomaly. We see that, since the signal is transmitted from and returns to the same point, all the exponentials due to the nodes between the sensing point and the anomaly location erase each other, and the first significant exponential is the one for $n=1$. ℓ_{eq_1} is actually the distance from the anomaly from the sensing point.

Moving to time domain, (30) becomes

$$\partial_{ch}^H(t) = \delta(t) * \mathbf{a}_0 * \delta(t) + \sum_{m=1}^{\infty} \delta \left(t - \sum_{n=1}^j p_n t_n \right) * \mathbf{a}_n * \delta \left(t - \sum_{n=1}^j p_n t_n \right), \quad (32)$$

where the peak at 0 is due to the bias introduced by the multiplication in (30), and the second peak is at t_a , associated to the distance ℓ_a of the anomaly from the receiver. A similar equation can be written starting from (31), but in this case t_a univocally identifies the distance of the anomaly from the sensing point. This information is in general more encrypted in the peak series of $\partial_{ch}(t)$. If the topology of the network is a-priori known, the position of the peaks can be related to a specific position in the network. More on this is discussed in [13].

ρ_{in} deserves a separate treatment. In fact, its values can be greater or lower than 0 and are often close to it. This means that at a certain frequency ρ_{in} can be greater than 0 and ρ_{in_a} can be lower. This might yield very high absolute values of ρ_a (see Fig. 4), but results in a distortion of the information about the anomaly. The resulting $\mathbf{r}_a(t)$ is in general rather jagged and difficult to analyze. For this reason it is not advisable to use the chain model when sensing ρ_{in} .

If we now consider again (17), (18) and (27), the anomaly can also be modeled using the superposition of the effects as an independent transfer function \mathbf{A}_S that adds to the unperturbed system (see Fig. (5)). This is the same model used in the radar literature for the detection of moving objects in cluttered

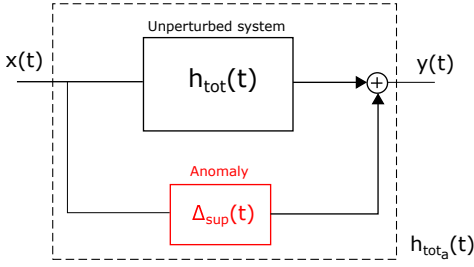


Fig. 5. Model of the anomaly using the superposition of the effects.

environments [22], [23], [24]. Relying on this model, the effect of the anomaly on the system can be derived by subtracting \mathbf{H}_{tot} from $\mathbf{H}_{\text{tot}_a}$. Since $\mathbf{H}_{\text{tot}_a} = \Delta_{ch}^H \mathbf{H}_{\text{tot}}$, and Δ_{ch}^H can be written as

$$\Delta_{ch}^H = \sum_{m=1}^{\infty} \mathbf{B}_m e^{-\Gamma \mathbf{e}_{q_m} \ell \mathbf{e}_{q_m}}, \quad (33)$$

we have

$$\Delta_{sup}^H = (\Delta_{ch}^H - \mathbf{I}) \mathbf{H}_{\text{tot}} = \sum_{k=1}^{\infty} \mathbf{C}_k e^{-\Gamma \mathbf{e}_{q_k} \ell \mathbf{e}_{q_k}}. \quad (34)$$

The reflectometry case is similarly derived. We see from (34) that all the exponential functions of (27) are still present, but their amplitude is modified by the effect of Δ_{ch}^H . All the exponential functions relative to the position of the anomaly are also added up in the sum. (34) can be further normalized by multiplication with $\mathbf{H}_{\text{tot}}^{-1}$, so that

$$\Delta_{supN}^H = \Delta_{sup}^H \mathbf{H}_{\text{tot}}^{-1} = \Delta_{ch}^H - \mathbf{I}, \quad (35)$$

which is basically the percentage variation of the measured CTF due to the anomaly. In time domain, (34) becomes

$$\partial_{sup}^H(t) = (\partial_{ch}^H(t) - \delta(t)) * \mathbf{h}_{\text{tot}}(t), \quad (36)$$

which includes all the peaks of $\mathbf{h}_{\text{tot}}(t)$ plus the new peaks generated by the fault. This can be also intuitively derived by considering that in the anomalous condition the test signal, which travels from the transmitter to a far receiver, is already modified by the anomaly before reaching the receiver. Therefore, already the first peak at the receiver is modified by the anomaly with respect to the unperturbed situation.

The reflectometry case is rather different when considering the superposition model. In fact, the test signal is sent and returns to the same point. The effect of an anomaly would therefore not influence the transitory until the transmitter signal has reached the anomaly. This means that all the possible peaks that occur before the anomaly are canceled out when computing $\mathbf{Y}_{\text{in}} - \mathbf{Y}_{\text{in}_a}$.

Hence, although the chain model and the superposition model are in principle different, they provide the same information about the effect of an anomaly, when considering the reflectometry case. In the end-to-end transmission case instead, the two models yield different results. In the chain model, all the first part of the transmission is canceled out, so that the first peak in time domain identifies the distance of the anomaly

from the closest node, while the superposition model features a trace with the same peak positions of the unperturbed situation, plus a series of peaks due to the anomaly.

We see here that, although both the end-to-end and reflectometric sensing approaches can be used to detect the presence of an anomaly, the location of the same is easier using the reflectometric approach, since the first peak of $\partial_{ch}^Y(t)$ or $\partial_{sup}^Y(t)$ already provides the distance of the anomaly from the sensing point.

B. Effect of concentrated faults and load impedance changes

A fault can be described electrically as a concentrated impedance branched to the network at the point where it occurs. Many models have been described in the literature (see [25], [26] and references therein) to best describe with lumped elements the dynamic evolution of different type of faults. In this paper, we will more generically consider faults with generic spectra.

A load impedance change can be due to two reasons: a stable variation of the load or a cyclic impedance variation due to the presence of active power converters.

From an electrical point of view, faults and impedance changes produce the same effect on the channel, since they are both concentrated and introduce the additional transfer function \mathbf{A} of (29) in the system. However, conversely from an impedance change, a fault modifies the topological structure of the network by introducing a new node with the fault impedance as a load (see Fig. 2). The consequence is that an impedance change is always localized at the same position of a previously known peak, and the same holds for all the following peaks of \mathbf{H}_a . On the other hand, all the peaks generated by a fault are new with respect to the unperturbed system. In Figure 6, the difference between a fault and a load impedance change is shown in the simple case of a single transmission line. Impedance measurements and the superposition model are used to derive the plots. The frequency domain plot shows that a load impedance change simply modifies the amplitude of \mathbf{Y}_{in} , especially at low frequencies. Conversely, a fault introduces a new oscillating mode that sums up to the exponential decaying trend, as explained in Section III-A. The time domain plot confirms that faults actually introduce new peaks with respect to the unperturbed situation, while load impedance changes simply modify their amplitude.

C. Effect of distributed faults

Distributed faults involve the damage of an extended section of a cable. Such faults can be due to exposure to bad weather conditions, water leakage in insulated cables, physical stress or other causes. The final effect is that the electrical properties of the damaged cable section change, resulting in different values of \mathbf{Y}_C and Γ . In such a case, \mathbf{A} is not simply an extra transfer function added to the system, but a modified version of the \mathbf{H}_n relative to the damaged section. Hence, supposing that the cable is uniformly damaged, a distributed fault causes two new discontinuities, one at the beginning and one at the end of the damaged section, which in turn results in a new series of peaks in the time domain response.

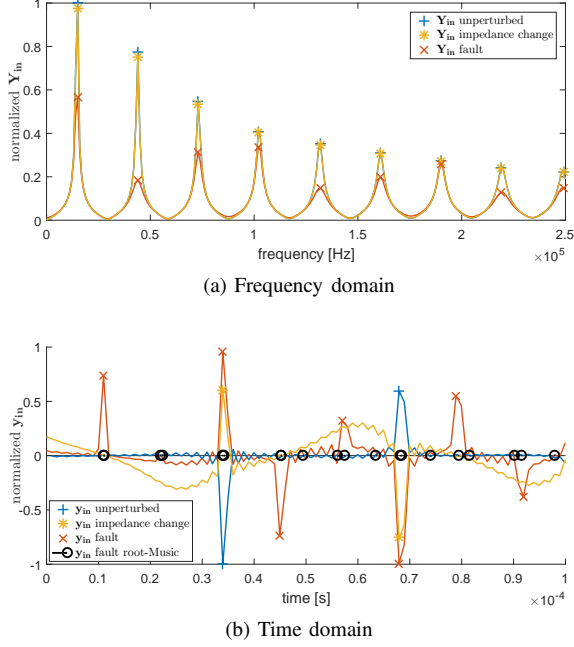


Fig. 6. Y_{in} simulated in presence of a fault and a load impedance change in frequency (a) and time (b) domain.

Considering again (26) and assuming the block $H_{j,0}$ to be uniformly damaged, $Y_{C_{j,0}}$, $\rho_{L_{j,0}}$ and $\Gamma_{j,0}$ change w.r.t. the unperturbed condition. The first two parameters cause, as concentrated faults, two new discontinuities: one at the beginning and one at the end of the damaged section, which in turn result in a new series of peaks in the time domain response. Like for the concentrated fault case, this causes in frequency domain the presence of an additional oscillating mode, its effect being more evident at low frequencies. On the other hand, since variations of $\Gamma_{j,0}$ act on a series of exponential functions which depend also on $\ell_{j,0}$, they modify the previously existing propagation modes of the signal. This results both in frequency and in time domain in a shift of the local peaks, particularly at high frequencies. The effect of a distributed fault on a single transmission line is shown in Figure 7.

Finally, distributed faults can be distinguished from concentrated faults from their effect on the channel characteristics. Namely, distributed faults introduce new propagation modes as concentrated faults do, but also modify the existing ones. This difference is taken into account in the algorithms presented in [13]. We also remark that, while the effect of concentrated faults is more evident at low frequencies, that of distributed faults is more evident at high frequencies. Therefore, either different frequency ranges or highly broadband signals should be used to sense the presence of both of them.

D. Influence of the position of the anomaly

The values of Δ_{ch} and Δ_{sup} depend on many factors, among which the severity of the anomaly, its position inside the network, the load values, the characteristics of the cables. It is not forcefully said that a more severe anomaly or an anomaly located closer to the receiver would produce

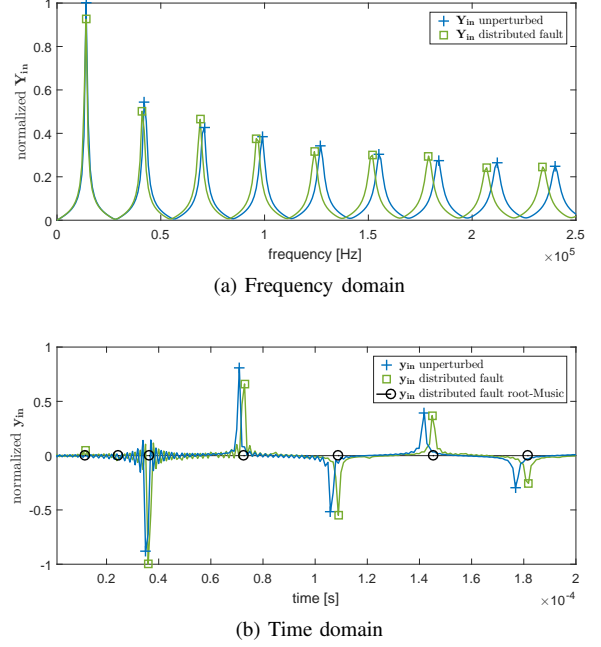


Fig. 7. Y_{in} simulated in presence of a distributed fault in frequency (a) and time (b) domain.

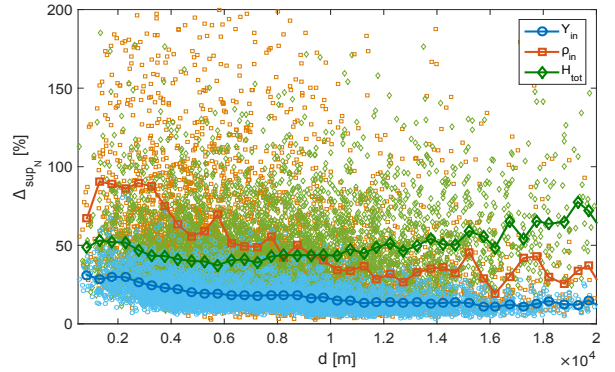


Fig. 8. Effect of the distance d of the anomaly from the receiver on Δ_{sup_N} .

higher values of Δ_{ch} . Its values depends on other factors too. However, we can state that, statistically, high values of Δ_{ch} and Δ_{sup} are expected for severe anomalies or high values of the load impedances. The effect of the location of the anomaly deserves a deeper analysis, that has been carried out by computing Δ_{sup_N} for 10000 simulated networks affected by a randomly located fault. For the details about the simulator please refer to [13]. No noise has been considered in this case.

Fig. 8 shows that both $\Delta_{sup_N}^{rho}$ and $\Delta_{sup_N}^Y$ have an average declining trend with the distance d of the fault from the transmitter. This comes from the fact that the amplitude of an echo signal naturally decreases with the traveled distance. We also notice that, while the realizations of $\Delta_{sup_N}^Y$ are rather close to the average, those of $\Delta_{sup_N}^{rho}$ are more scattered. This is due to the fact that often the values of ρ_{in} are close to 0 (see explanation in Section III-A).

More notably, Fig. 8 shows that the values of $\Delta_{sup_N}^H$, after an initial decrease, tend to increase again. We point out that we

set the transmitter of the end-to-end signal to be as far away as possible from the receiver. This means that low values of d correspond to faults located next to the receiver, while high values of d correspond to faults located next to the transmitter. This means that a fault or, more in general, any anomaly located either close to the transmitter or to the receiver, yields higher values of Δ_{supN}^H compared to an anomaly located in the middle of the network. To explain this fact, we rely again on the symmetry of the end-to-end signals (see Theorem 1). Since the signal is unidirectional, an anomaly located close to the transmitter would significantly modify it, but the result would be smoothed out by the rest of the propagation path. Conversely, an anomaly located close to the receiver acts on an already damped signal, but the results gets to the receiver without further smoothing. Anomalies located in the middle of the network suffer from both a weak incident signal and a smoothed resulting signal delivered to the receiver.

IV. CONCLUSIONS

In this paper, we presented a thorough analysis of what kind of information can be retrieved about a power line network by using high-frequency signals, such as those generated by power line modems. The proposed approach enables to retrieve information about the network topology, the aging of the cables, the variation of a load, the presence of a fault. We provided closed-form formulas for the input impedance and reflection coefficient at one node as well as for the CTF. We then presented two different models, namely chain and superposition, to represent the occurrence of a generic anomaly in the network. We showed how these models can be applied to both reflectometric and end-to-end sensing, and discussed the different results that they can provide. We finally presented how different kind of anomalies, namely a lumped fault, an impedance variation and a distributed fault, affect the propagation of signals and discussed how it is possible to distinguish between them using remote single-ended or double-ended sensing. The interested reader may also read [13], where a complete measurement set-up to be included in PLC modems and different algorithms are presented to automatically detect, classify and locate electrical anomalies.

REFERENCES

- [1] A. von Meier, E. Stewart, A. McEachern, M. Andersen, and L. Mehrmanesh, "Precision micro-synchrophasors for distribution systems: A summary of applications," *IEEE Transactions on Smart Grid*, vol. 8, no. 6, pp. 2926–2936, Nov 2017.
- [2] S. Galli, A. Scaglione, and Z. Wang, "For the grid and through the grid: The role of power line communications in the smart grid," *Proceedings of the IEEE*, vol. 99, no. 6, pp. 998–1027, June 2011.
- [3] C. Cano, A. Pittolo, D. Malone, L. Lampe, A. M. Tonello, and A. G. Dabak, "State of the art in power line communications: From the applications to the medium," *IEEE Journal on Selected Areas in Communications*, vol. 34, no. 7, pp. 1935–1952, July 2016.
- [4] S. Galli and D. L. Waring, "Loop makeup identification via single ended testing: beyond mere loop qualification," *IEEE Journal on Selected Areas in Communications*, vol. 20, no. 5, pp. 923–935, Jun 2002.
- [5] C. Neus, "Reflectometric analysis of transmission line networks," Ph.D. dissertation, Vrije Universiteit Brussel, 2011.
- [6] F. Lindqvist, "Estimation and detection of transmission line characteristics in the copper access network," Ph.D. dissertation, Lund University, 2011.

- [7] M. Sedighizadeh, A. Rezazadeh, and I. Elkalashy, "Approaches in high impedance fault detection – a chronological review," *Advances in Electrical and Computer Engineering*, vol. 10, no. 3, pp. 114–128, 2010.
- [8] K. Jia, T. Bi, Z. Ren, D. W. P. Thomas, and M. Sumner, "High frequency impedance based fault location in distribution system with dgs," *IEEE Transactions on Smart Grid*, vol. 9, no. 2, pp. 807–816, March 2018.
- [9] F. Passerini and A. M. Tonello, "Full duplex power line communication modems for network sensing," in *2017 IEEE International Conference on Smart Grid Communications (Smartgridcomm)*, October 2017.
- [10] A. N. Milioudis, G. T. Andreou, and D. P. Labridis, "Enhanced protection scheme for smart grids using power line communications techniques – part II: Location of high impedance fault position," *IEEE Transactions on Smart Grid*, vol. 3, no. 4, pp. 1631–1640, Dec 2012.
- [11] A. M. Pasdar, Y. Sozer, and I. Husain, "Detecting and locating faulty nodes in smart grids based on high frequency signal injection," *IEEE Transactions on Smart Grid*, vol. 4, no. 2, pp. 1067–1075, June 2013.
- [12] C. R. Paul, *Analysis of Multiconductor Transmission Lines*, 2nd ed. Wiley-IEEE Press, 2007.
- [13] F. Passerini and A. M. Tonello, "Smart grid network sensing using power line modems: A framework for anomaly detection and localization," *Submitted to IEEE Transactions on Smart Grids*, 2018.
- [14] F. Versolatto and A. Tonello, "An MTL theory approach for the simulation of MIMO power-line communication channels," *IEEE Transactions on Power Delivery*, vol. 26, no. 3, pp. 1710–1717, 2011.
- [15] P. D. B. Ronald E. Miller, *Input-Output Analysis: Foundations and Extensions - 2nd edition*, 2nd ed. Cambridge University Press, 2009.
- [16] P. I. Somlo and J. D. Hunter, "Condition for reflection coefficient magnitude greater than one for passive transmission line and passive load," *IEEE Transactions on Instrumentation and Measurement*, vol. IM-30, no. 3, pp. 230–231, Sept 1981.
- [17] A. M. Tonello, F. Versolatto, B. Béjar, and S. Zazo, "A fitting algorithm for random modeling the plc channel," *IEEE Transactions on Power Delivery*, vol. 27, no. 3, pp. 1477–1484, Jul. 2012.
- [18] P. Stoica and R. Moses, *Spectral Analysis of Signals*. Pearson Prentice Hall, 2005. [Online]. Available: <https://books.google.at/books?id=h78ZAQAIAAJ>
- [19] M. Ahmed and L. Lampe, "Parametric and nonparametric methods for power line network topology inference," in *Power Line Communications and Its Applications (ISPLC), 2012 16th IEEE International Symposium on*, March 2012, pp. 274–279.
- [20] A. Tonello and F. Versolatto, "Bottom-up statistical PLC channel modelling - part I: Random topology model and efficient transfer function computation," *IEEE Transactions on Power Delivery*, vol. 26, no. 2, pp. 891–898, Apr. 2011.
- [21] A. Codino, Z. Wang, R. Razzaghi, M. Paolone, and F. Rachidi, "An alternative method for locating faults in transmission line networks based on time reversal," *IEEE Transactions on Electromagnetic Compatibility*, vol. 59, no. 5, pp. 1601–1612, Oct 2017.
- [22] S. Kay, "Optimal signal design for detection of gaussian point targets in stationary gaussian clutter/reverberation," *IEEE Journal of Selected Topics in Signal Processing*, vol. 1, no. 1, pp. 31–41, June 2007.
- [23] M. Soltanalian, "Signal design for active sensing and communications," Ph.D. dissertation, Uppsala University, 2014.
- [24] L. Abboud, "Time reversal techniques applied to wire fault detection and location in wire networks," Ph.D. dissertation, SUPELEC - Univ Paris-Sud, 2013.
- [25] S. Maximov, V. Torres, H. F. Ruiz, and J. L. Guardado, "Analytical model for high impedance fault analysis in transmission lines," *Mathematical Problems in Engineering*, vol. 2014, 2014.
- [26] S. Gautam and S. M. Brahma, "Detection of high impedance fault in power distribution systems using mathematical morphology," *IEEE Transactions on Power Systems*, vol. 28, no. 2, pp. 1226–1234, May 2013.
- [27] S. Galli, "Exact conditions for the symmetry of a loop," *IEEE Communications Letters*, vol. 4, no. 10, pp. 307–309, Oct 2000.



Fig. 9. Example of a network with two sections and one load.

APPENDIX A

DERIVATION OF THE INPUT IMPEDANCE IN THE GENERAL CASE

In this Appendix, we show how (15) and (16) are derived starting from (9) and (10).

In Section II, we derived the Taylor series of \mathbf{Y}_{in} and ρ_{in} in the case of a single line with a load at the end. Here we first consider a MTL composed by two line sections of length ℓ_1 and ℓ_2 with no load at the junction and a load at the end (see Fig. 9), derive \mathbf{Y}_{in} and ρ_{in} and finally derive by induction.

The problem of finding \mathbf{Y}_{in} and ρ_{in} for the network depicted in Fig. 9 reduces to the problem of finding ρ_1 , which is the equivalent load reflection coefficient relative to the first line section. Then (9) and (10) can be applied using ρ_1 instead of (3). ρ_1 is also the input reflection coefficient w.r.t. the second line, therefore we can write

$$\rho_1 = \mathbf{N}_2 \mathbf{T}_2 \left[\rho_{12}^{\text{M}} + (\mathbf{I} - \rho_{\text{G}}^{\text{M}} \rho_{\text{G}}^{\text{M}}) \rho_{\text{B}2}^{\text{M}} \right] \mathbf{T}_2^{-1} \mathbf{N}_2^{-1} + \mathbf{N}_2 \mathbf{T}_2 \left[(\mathbf{I} - \rho_{12}^{\text{M}} \rho_{12}^{\text{M}}) \rho_{\text{B}2}^{\text{M}} \sum_{n=1}^{\infty} (-1)^n (\rho_{\text{B}2}^{\text{M}})^n \right] \mathbf{T}_2^{-1} \mathbf{N}_2^{-1} \quad (37)$$

where $\rho_{12}^{\text{M}} = \mathbf{T}^{-1} \mathbf{Y}_{\text{C}2} (\mathbf{Y}_{\text{C}2} + \mathbf{Y}_{\text{C}1})^{-1} (\mathbf{Y}_{\text{C}2} - \mathbf{Y}_{\text{C}1}) \mathbf{Y}_{\text{C}2}^{-1} \mathbf{T}$, $\mathbf{N}_2 = (\mathbf{Y}_{\text{C}1} + \mathbf{Y}_{\text{C}2}) \mathbf{Y}_{\text{C}2}^{-1}$ and $\rho_{\text{B}2}^{\text{M}} = e^{-\Gamma_2 \ell_2} \rho_{\text{L}}^{\text{M}} e^{-\Gamma_2 \ell_2}$. We now substitute $\rho_{\text{L}}^{\text{M}}$ in (9) and (10) with ρ_1^{M} , thus obtaining

$$\mathbf{Y}_{\text{in}} = \mathbf{T}_1 \left[\mathbf{I} + 2e^{-\Gamma_1 \ell_1} \mathbf{O}_2 \rho_{12}^{\text{M}} \mathbf{O}_2^{-1} e^{-\Gamma_1 \ell_1} + 2e^{-\Gamma_1 \ell_1} \mathbf{O}_2 e^{-\Gamma_2 \ell_2} \rho_{\text{L}}^{\text{M}} e^{-\Gamma_2 \ell_2} \mathbf{O}_2^{-1} e^{-\Gamma_1 \ell_1} + 2 \sum_{n=2}^{\infty} \dots \right] \mathbf{T}_1^{-1} \mathbf{Y}_{\text{C}} \quad (38)$$

and

$$\rho_{\text{in}} = \mathbf{N}_1 \mathbf{T}_1 \left[\rho_{\text{G}1}^{\text{M}} + \mathbf{Q}_1 \left(e^{-\Gamma_1 \ell_1} \mathbf{O}_2 \rho_{12}^{\text{M}} \mathbf{O}_2^{-1} e^{-\Gamma_1 \ell_1} + e^{-\Gamma_1 \ell_1} \mathbf{O}_2 \mathbf{Q}_2 e^{-\Gamma_2 \ell_2} \rho_{\text{L}}^{\text{M}} e^{-\Gamma_2 \ell_2} \mathbf{O}_2^{-1} e^{-\Gamma_1 \ell_1} \right) + \sum_{n=1}^{\infty} \dots \right] \mathbf{T}_1^{-1} \mathbf{N}_1^{-1} \quad (39)$$

where $\mathbf{O}_2 = \mathbf{T}_2^{-1} \mathbf{N}_2 \mathbf{T}_2$ and $\mathbf{Q}_n = \mathbf{I} - \rho_{\text{G}n}^{\text{M}} \rho_{\text{G}n}^{\text{M}}$. Similarly to the single line case, (38) and (39) are composed by different terms. The first is a constant w.r.t. the line lengths that depends on the impedance mismatch between the source and the first line segment. Then two terms follow, which depend exponentially on $2\ell_1$ and on $2(\ell_1 + \ell_2)$ respectively. Finally, an infinite series follows (not explicitly written here) with terms that depend on multiples of $2\ell_1$, $2(\ell_1 + \ell_2)$ and combinations of these two terms.

The same reasoning can be extended by induction to lines composed by any number of segments, also with multiple segments branched to a single node, thus yielding the results expressed by (15) and (16).

APPENDIX B

PROOF OF THEOREM 1

We explained in Section II-B that the transfer function by any two points in a wired network is given by (26). We define now the backbone as the shortest path between the transmitter and the receiver nodes, that is either the line of sight path in wireless networks or the shortest sequence of line segments connecting the two ends in wired networks. We also define $\mathbf{H}_{\text{tot}}^{\text{A} \rightarrow \text{B}}$ and $\mathbf{H}_{\text{tot}}^{\text{B} \rightarrow \text{A}}$ as the transfer functions from A to B and from B to A respectively.

$\mathbf{H}_{\text{tot}}^{\text{A} \rightarrow \text{B}}$ can be computed using the carry-back method described in [14], which involves as first step carrying back all the loads at the termination nodes to the backbone. Since every signal from A to B or from B to A travels through the same backbone, this first step yields the same result also for $\mathbf{H}_{\text{tot}}^{\text{B} \rightarrow \text{A}}$. At this point the network has been reduced to a sequence of line segments with equivalent loads branched at every node. In the following step, the resulting \mathbf{H}_n matrices are multiplied with each other in order to give the total transfer function. It has already been demonstrated in [27] that if $\mathbf{Y}_{\text{R}}^{\text{A}} = \mathbf{Y}_{\text{R}}^{\text{B}} = \mathbf{Y}_{\text{L}}^{\text{A}} = \mathbf{Y}_{\text{L}}^{\text{B}}$, then $\mathbf{H}_{\text{tot}}^{\text{A} \rightarrow \text{B}} = \mathbf{H}_{\text{tot}}^{\text{B} \rightarrow \text{A}}$, otherwise the equality does not hold and in general the two transfer functions are not similar to each other. However, (26) shows that, apart from a multiplicative factor, the same exponentials are multiplied with each other in the case of $\mathbf{H}_{\text{tot}}^{\text{A} \rightarrow \text{B}}$ and $\mathbf{H}_{\text{tot}}^{\text{B} \rightarrow \text{A}}$, just in opposite order. When transforming (26) to time domain, this results in a sequence of smoothed peaks whose location is the same.